OXFORD CENTRE FOR COLLABORATIVE APPLIED MATHEMATICS

Report Number 10/07

Frost heave in compressible soils

by

Apala Majumdar, Stephen Peppin, Robert Style, Graham Sander

Oxford Centre for Collaborative Applied Mathematics
Mathematical Institute
24 - 29 St Giles'
Oxford
OX1 3LB
England

FROST HEAVE IN COMPRESSIBLE SOILS

APALA MAJUMDAR*, STEPHEN PEPPIN†, ROBERT STYLE‡, AND GRAHAM SANDER§

Abstract. We develop a mathematical model of frost heave in compressible soils based on a morphological instability of the ice–soil interface. The theory accounts for heave and soil consolidation, while avoiding the frozen fringe assumption. Using a Lie-Bäcklund transformation an analytical solution to the governing equations is found. Two solidification regimes occur: a compaction regime in which the soil consolidates to accommodate the ice lenses, and a heave regime during which the soil is fully consolidated and heaves. The rate of heave is found to be independent of the rate of freezing, consistent with field and laboratory observations.

Key words. frost heave, colloids, Lie-Backlund transformation

AMS subject classifications. 86A40, 86A99

1. Introduction. Frost heave is a phenomenon in which the ground surface deforms and *heaves* under the action of freezing and thawing. The process leads to challenging engineering problems in cold regions of Earth as well as to the development of peculiar geological features (patterned ground) [42]. In the early twentieth century it was discovered that frost heave is caused by the formation of repetitive layers of segregated ice in the soil, called *ice lenses* [37, 9]. The most natural explanation for heave – expansion of ice upon freezing – has surprisingly little effect. The negligible importance of ice expansion was demonstrated definitively by Taber [37] and Zhu *et al.* [44] who showed that frost heave occurs in soils saturated with benzene and argon, materials which *contract* upon freezing. Rather, the heave occurs because the water which forms the ice lenses is drawn from other regions of the soil, and the frozen part comes to contain an excess mass of ice. The amount of heave is strongly correlated with the volume of ice lenses formed [37, 42].

Mathematical models of frost heave tend to adopt the frozen fringe assumption [23, 24, 12, 18, 34]. A partially frozen region of soil is assumed to exist ahead of (*i.e.* at temperatures warmer than) the warmest ice lens. A combination of factors allow the partially frozen soil to segregate, revealing a new lens of pure ice [23, 34]. Remarkably, frost heave experiments on highly compressible soils such as kaolinite, bentonite and silica microspheres found that there is no pore ice in the soil near the ice lenses [5, 6, 39, 40]. These results confirm early observations of Beskow that in clays and fine silts the soil between ice lenses is soft and unfrozen [4, 25], but have yet to be explained theoretically.

Recently it has been suggested that ice lens formation in such systems may be due to a morphological instability of the ice–soil interface [27]. In the present work we build on this approach to develop a continuum theory of frost heave in compressible soils that does not depend on the frozen fringe assumption. The model bears some similarity to mushy layer models of alloy solidification [16, 43], in that we treat the mixed-phase region (ice lenses + soil) as a continuum, rather than attempt to track individual ice crystals. In section 2 we discuss the phase diagram of a soil, distinguishing between segregational freezing (ice lenses) and interstitial freezing (pore ice). The frost heave model is presented in section 3. An analytical solution of the model

*OCCAM, Mathematical Institute, University of Oxford, OX1 3LB.
†OCCAM, Mathematical Institute, University of Oxford, OX1 3LB.
‡OCCAM, Mathematical Institute, University of Oxford, OX1 3LB.
§Department of Civil and Building Engineering, Loughborough University, LE11 3TU.

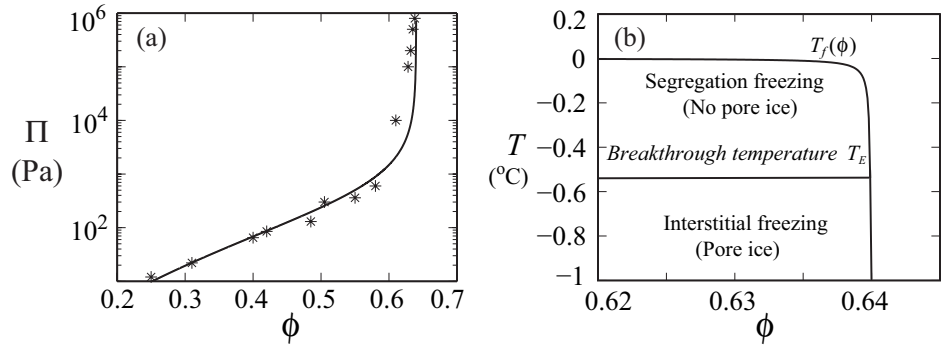

FIG. 2.1. *(a) Measurements of the osmotic pressure of an aqueous suspension of silica spheres (radius 0.5 μm) [14], along with a fit to the data using (2.2) with $a_1 = 5.5 \times 10^3$, $a_2 = 3.7 \times 10^3$, $a_3 = 1.3 \times 10^5$ $a_4 = -8.7 \times 10^4$. (b) Phase diagram of an aqueous suspension of silica spheres, showing the freezing temperature $T_f(\phi)$ and the breakthrough temperature T_E.*

equations is obtained in section 4, while in section 5 we present results and comparison with experiment.

2. Segregational and interstitial freezing. During the solidification of soils two distinct types of freezing processes occur [17]. *Segregational freezing* involves macroscopic regions of ice segregating from the soil matrix. In contrast, *interstitial freezing* occurs when ice enters the pores of the soil. At relatively fast freezing rates the transition from segregational to interstitial freezing occurs via nonequilibrium particle trapping effects [38, 33]. As noted by Jackson *et al.* [17], in soils experiencing significant frost heave the freezing rates are typically slow enough that particle trapping does not occur. In this case the equilibrium phase diagram of a soil determines conditions under which the soil experiences segregational or interstitial freezing. In the following we determine the phase diagram of a soil composed of spherical silica particles, such as those used by Watanabe *et al.* [40, 41].

The segregation freezing temperature $T_f(\phi)$ (analogous to the liquidus temperature in alloys) is a function of the particle volume fraction ϕ, and is given by the equation

$$T_f(\phi) = T_m \left(1 - \frac{\Pi(\phi)}{\rho_l L_f}\right), \tag{2.1}$$

where T_m is the freezing temperature of pure water, $\Pi(\phi)$ is the osmotic pressure of the particles, ρ_l the density of water and L_f is the latent heat of fusion [22], [27]. Figure 2.1a shows measurements of $\Pi(\phi)$ for silica spheres of radius $R = 0.5\,\mu$m [14]. The solid line is a fit to the data using the equation [28]

$$\Pi(\phi) = \frac{\phi k_B T_m}{v_p} \frac{1 + \sum_{k=1}^{n} a_k \phi^k}{1 - \phi/\phi_p}, \tag{2.2}$$

where k_B is Boltzmann's constant, $v_p = \frac{4}{3}\pi R^3$ is the particle volume, $\phi_p = 0.64$ is the volume fraction at close packing, the a_k are constants and n is chosen large enough to yield a good fit (usually $n = 4$ is sufficient).

Figure 2.1b shows the freezing temperature $T_f(\phi)$ calculated from (2.1). When the temperature is lowered below T_m ice first forms outside of the soil pores as segregated ice. At a given temperature the concentration ϕ of the soil in equilibrium with

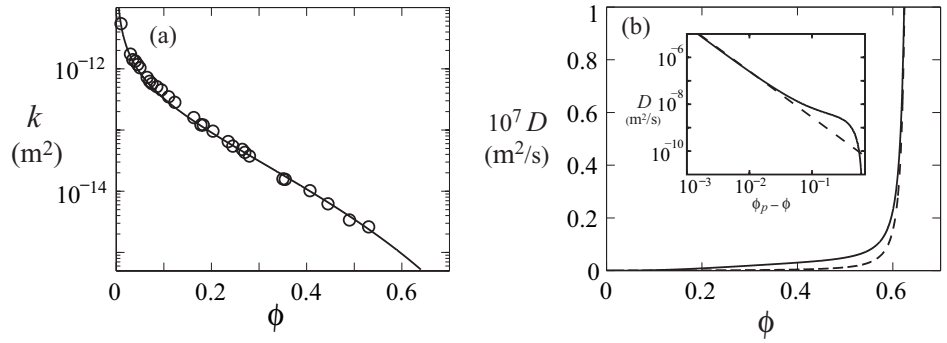

FIG. 2.2. *(a) Measurements of the permeability $k(\phi)$ of a suspension of silica spheres [11] along with a fit of the data to the equation $k = (2R^2/9\phi)(1-\phi)^5$. (b) Diffusivity of a suspension of silica spheres calculated using the Stokes-Einstein equation (2.4) (solid line) and the simpler equation (4.1) (dashed line). The inset shows the diffusivity plotted versus $\phi_p - \phi$.*

pure ice is dictated by the $T_f(\phi)$ curve. Eventually the soil becomes fully consolidated ($\phi \to \phi_p$) and a critical ice *breakthrough* temperature T_E is reached [6, 36]. At this temperature ice enters the pore space between particles, and interstitial freezing proceeds. The breakthrough temperature can be estimated from the pressure difference required for ice to enter the pore space. Thus, for close-packed spherical particles breakthrough occurs when $\Pi = \gamma/R_p$, where γ is the ice-water surface energy and R_p is the effective pore radius. For a hexagonally close-packed system with zero contact angle between the ice-water and water-particle interfaces, Hilden *et al.* [15] obtain $R_p = R/11$. Inserting this expression for Π into (2.1) gives

$$T_E = T_m \left(1 - \frac{11\gamma}{\rho_l L_f R}\right). \tag{2.3}$$

Using typical values for ice ($\gamma = .03\,\mathrm{J/m^2}$, $\rho_l = 10^3\,\mathrm{kg/m^3}$ and $L_f = 3.3 \times 10^5\,\mathrm{J/kg}$) gives $T_E = T_m - 0.54\,^\circ\mathrm{C}$ (figure 2.1b).

The soil diffusivity $D(\phi)$ can be determined from the Stokes-Einstein relation [35, 28]

$$D(\phi) = \phi \frac{k(\phi)}{\eta} \left(\frac{\partial \Pi(\phi)}{\partial \phi}\right), \tag{2.4}$$

where $k(\phi)$ is the permeability and η the fluid viscosity. Davis *et al.* [11] have measured the dimensionless permeability $\hat{k} = 9\phi k/2R^2$ and their data can be fit well to the expression $\hat{k} = (1-\phi)^5$, as shown in figure 2.2a. The diffusivity calculated from (2.4) is shown as the solid line in figure 2.2b.

3. 1D model. We develop a model of the unidirectional solidification system studied by Watanabe *et al.* [40, 41]. In their experiments a soil of initial particle fraction ϕ_0 is pulled at a constant rate V through a fixed temperature gradient G_T (figure 3.1). We consider a coordinate system fixed with respect to the isotherms, and define the $z = 0$ position as the $0\,^\circ\mathrm{C}$ isotherm. The temperature profile in the system is then given by the linear relation

$$T(z) = T_m + G_T z. \tag{3.1}$$

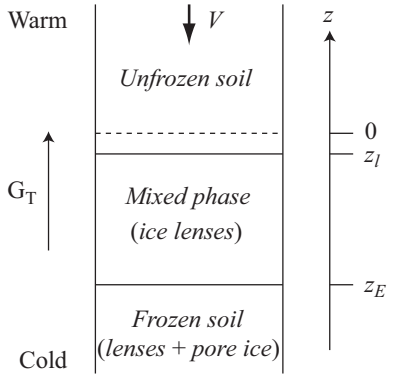

FIG. 3.1. *Schematic diagram of the solidification cell used by Watanabe (2002). The sample is moved at a fixed rate V through a constant temperature gradient G_T. Ice enters the pores at z_E while z_l demarcates the boundary between the mixed-phase region and unfrozen soil.*

If V is sufficiently small a single planar ice lens pushes the soil ahead indefinitely [5, 40, 29]. At faster rates segregated ice forms in the soil interior yielding a mixed phase region composed of ice lenses and unfrozen soil [5, 29]. We treat this region as a continuum characterized by an average segregated-ice volume fraction χ, and so the overall particle fraction in this region is $(1-\chi)\phi$. The boundary between the unfrozen soil and the mixed-phase region is denoted by z_l. Similarly to mushy layer models of alloy solidification we assume that the mixed phase region is locally in equilibrium [43], so that the particle concentration in the soil phase ϕ and the temperature T are coupled by the phase diagram. The temperature at z_l is then $T_l = T_f(\phi_l)$. From figure 2.1b it is evident that for most of the range in ϕ the freezing temperature $T_f(\phi)$ is very near to T_m. Over this range we can make the approximation $T_l = T_m$. The position of the mixed-phase boundary is then given by

$$z_l = 0. \tag{3.2}$$

Using (2.3) and (3.1) the breakthrough position z_E at which ice enters the pores is obtained as

$$z_E = -\frac{11 T_m \gamma}{\rho_l L_f R G_T}. \tag{3.3}$$

In order to predict heave it is necessary to consider conservation of mass in the system. In the mixed-phase region $0 > z > z_E$, ϕ is coupled to the temperature T by the phase diagram and is therefore known. We neglect all mass transport in the frozen region $z < z_E$ where the temperatures are below T_E. Thus we have only to find $\phi(z,t)$ in the region $z > 0$. As mentioned in the introduction the expansion of ice on freezing is not essential to the frost heave phenomenon and we ignore it here. In the experiments of Watanabe *et al.* [40, 41] the cell was oriented horizontally and the effects of gravity were negligible. Therefore the difference in density between the water and soil particles can also be safely ignored.

Given these approximations, in a frame of reference fixed with respect to the isotherms, conservation of mass in the region $z > 0$ can be written as

$$\frac{\partial \phi}{\partial t} = \frac{\partial}{\partial z}\left(D(\phi)\frac{\partial \phi}{\partial z} + V\phi \right), \tag{3.4}$$

with boundary conditions

$$\chi\phi V = -D(\phi)\frac{\partial\phi}{\partial z}, \qquad (z = 0), \tag{3.5}$$

$$\phi \to 0, \qquad (z \to \infty). \tag{3.6}$$

The first boundary condition (3.5) expresses conservation of mass at the mixed-phase/unfrozen-soil boundary. When the ice fraction χ at $z = 0$ is 1 all the soil is pushed ahead by a single stable ice lens. When $\chi < 1$ multiple ice lenses form, yielding a mixed-phase region. The second boundary condition (3.6) ensures that a reservoir of pure water is available to keep the soil saturated. The initial condition is that of a layer of soil of height L and concentration ϕ_0, above which is the water reservoir:

$$\phi(z, 0) = \begin{cases} \phi_0, & 0 < z \le L \\ 0, & z > L. \end{cases} \tag{3.7}$$

3.1. Marginal stability. Equations (3.4)–(3.7) contain the unknown ice fraction χ. One possible closure equation to obtain χ is a marginal stability condition [20] given by

$$MG_T = G_{T_f} \qquad (z = 0), \tag{3.8}$$

where $G_{T_f} = \partial T_f(\phi)/\partial z$ is the freezing temperature gradient at $z = 0$ and M, the morphological number, is assumed constant. When $M > 1$ a supercooled region of soil exists ahead of the interface [30]. In mushy layer models of alloy solidification, it is usually assumed that $M = 1$ at the boundary [43] (marginal equilibrium). That is, the mushy layer grows just enough to ensure supercooling does not occur. Here we assume that M equals some critical value M_c that may deviate from 1. Conservation of mass at the interface (3.5) along with (2.4) and (2.1) implies that $\chi\phi V = -D\partial\phi/\partial z = \phi k\rho_l L_f G_{T_f}/\eta T_m$ or equivalently

$$\chi = \frac{M_c\rho_l L_f G_T k}{T_m \eta V}. \tag{3.9}$$

Since M_c is assumed constant (3.9) suggests that $\chi \sim V^{-1}$. This scaling is shown in figure 3.2, along with experimental data. The data can be fit to the expression

$$\chi = \frac{V_c}{V}, \tag{3.10}$$

where V_c is a critical freezing rate above which the interface becomes unstable. In Watanabe's experiments [41], $V_c = 0.15\,\mu$m/s, $G_T = 190\,^\circ$C/m and $R = 1.1\,\mu$m. Comparison of (3.10) and (3.9) gives $M_c \sim 10^{-2}$, suggestive of a subcritical instability, in the sense that $M_c < 1$ [27].

4. Solution via Lie-Bäcklund transformation. In order to find analytical solutions to the system (3.4)–(3.8) we replace (2.4) with a diffusivity of the form

$$D(\phi) = \frac{D_0}{(1 - \phi/\phi_p)^2}, \tag{4.1}$$

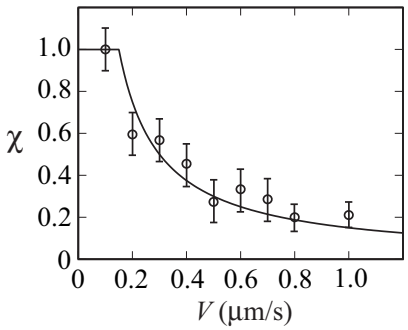

FIG. 3.2. *Plot of the ice fraction χ versus the pulling speed V measured by Watanabe [41]. The ice fraction is calculated as $\chi = l_{th}/(l_{th} + l_{sp})$, where l_{th} and l_{sp} are, respectively, the measured thicknesses of and spacings between the ice lenses.*

where $D_0 = 6.0 \times 10^{-11} \mathrm{m}^2/\mathrm{s}$ is a constant. This expression, plotted as the dashed line in figure 2.2b, captures the essential limiting behaviours that D approaches a constant in the dilute limit and diverges in the limit of a rigid porous medium [35, 28]. In [27] we worked in the low-concentration regime where the diffusivity is approximately a constant. In this paper, we are interested in the close-packing limit and as can be seen from figure 2.2b, (4.1) shows good agreement with the exact expression (2.4) in the close-packing regime $\phi \to \phi_p$.

We nondimensionalise the governing equations by introducing the variables $\hat{z} = z/L$, $\hat{t} = tD_0/L^2$ and $\Phi = \phi/\phi_p$ into equations (3.4)–(3.7) to give, upon dropping the carets,

$$\frac{\partial \Phi}{\partial t} = \frac{\partial}{\partial z}\left[\frac{1}{(1-\Phi)^2}\frac{\partial \Phi}{\partial z} + Pe\Phi\right], \tag{4.2}$$

$$\chi \Phi Pe + \frac{1}{(1-\Phi)^2}\frac{\partial \Phi}{\partial z} = 0, \qquad (z = 0), \tag{4.3}$$

$$\Phi \to 0, \qquad (z \to \infty), \tag{4.4}$$

$$\Phi(z,0) = \begin{cases} \Phi_0, & 0 < z \leq 1 \\ 0, & z > 1 \end{cases} \tag{4.5}$$

where $Pe = VL/D_0$ is the Peclet number and $\Phi_0 = \phi_0/\phi_p$.

In the case $\chi = 1$ a Lie-Bäcklund transformation [32] can be used to obtain an analytical solution for the system (4.2)–(4.5). This method is particularly useful for obtaining exact analytical solutions with nonlinear diffusivity and conductivity functions and such solutions provide a demanding test of numerical simulations [13, 2, 3]. In what follows we set $\chi = 1$ and derive the corresponding Lie-Bäcklund analytical solution. We note in passing that equations (4.2)–(4.5), in the case $\chi = 1$, are employed by Davis and Russel [10] in their study of ultrafiltration and hence this method yields an analytical solution to that problem as well.

We introduce a change of variable and define

$$\Phi^*\left(z^*(z,t),t\right) = \frac{1}{1-\Phi}$$
$$z^* = \int_0^z 1 - \Phi(z',t)\, dz'. \tag{4.6}$$

Then

$$\Phi = 1 - \frac{1}{\Phi^*}$$

and

$$\frac{\partial z^*}{\partial z} = \frac{1}{\Phi^*\left(z^*, t\right)},$$

$$\frac{\partial z^*}{\partial t} = -\int_0^z \frac{\partial \Phi}{\partial t}(z^{'}, t)\, dz^{'} = -\frac{1}{\Phi^*}\Phi^*_{z^*} - \frac{Pe}{\Phi^*}\left(\Phi^* - 1\right).$$

We use the chain rule and the definitions (4.6) to obtain the following:

$$\frac{\partial \Phi}{\partial t} = \frac{1}{\Phi^{*2}}\left[\Phi^*_{z^*}\frac{\partial z^*}{\partial t} + \frac{\partial \Phi^*}{\partial t}\right] = -\frac{(\Phi^*_{z^*})^2}{(\Phi^*)^3} - \frac{Pe}{(\Phi^*)^3}\Phi^*_{z^*}\left(\Phi^* - 1\right) + \frac{\Phi^*_t}{(\Phi^*)^2} \quad (4.7)$$

and

$$\frac{\partial}{\partial z}\left[\frac{1}{(1-\Phi)^2}\Phi_z + Pe\Phi\right] = \frac{1}{\Phi^*}\frac{\partial}{\partial z^*}\left[\frac{\Phi^*_{z^*}}{\Phi^*} + Pe\frac{1}{\Phi^*}\left(\Phi^* - 1\right)\right]. \quad (4.8)$$

Substituting (4.7) and (4.8) into (4.2), the governing partial differential equation for the transformed variable Φ^* becomes

$$\frac{\partial \Phi^*}{\partial t} = \frac{\partial}{\partial z^*}\left[\Phi^*_{z^*} + Pe\left(\Phi^* - 1\right)\right]. \quad (4.9)$$

The boundary condition on $z = 0$ can be transformed similarly and the statement of the transformed problem is thus given by

$$\begin{aligned}
&\frac{\partial \Phi^*}{\partial t} = \frac{\partial}{\partial z^*}\left[\Phi^*_{z^*} + Pe\left(\Phi^* - 1\right)\right] \\
&\Phi^*_{z^*} + Pe\left(\Phi^* - 1\right) = 0 \quad \text{on } z^* = 0 \\
&\Phi^* \to 1 \quad z^* \to \infty \\
&\Phi^*(z^*, 0) = \begin{cases} \frac{1}{1-\Phi_0}, & 0 < z^* \le 1 - \Phi_0, \\ 1, & z^* > 1 - \Phi_0. \end{cases}
\end{aligned} \quad (4.10)$$

(since $z = \int_0^{z^*} \Phi^*(z^{'}, t)\, dz^{'}$).

The partial differential equation for Φ^* can be transformed into the heat equation using a second change of variable (see [8] for similar examples in the context of Richards' equation with arbitrary time-dependent surface fluxes) by choosing

$$\begin{aligned}
&Z = Pez^*; \quad T = Pe^2 t \\
&\bar{\phi}(Z, T) = \left(\Phi^* - 1\right)\mathrm{e}^{\frac{Z}{2} + \frac{T}{4}}
\end{aligned} \quad (4.11)$$

Then the system (4.10) is reduced to the following initial-boundary value problem for the heat equation:

$$\begin{aligned}
&\bar{\phi}_T = \bar{\phi}_{ZZ} \\
&\bar{\phi}_Z + \frac{\bar{\phi}}{2} = 0 \quad Z = 0 \\
&\bar{\phi} \to 0 \quad Z \to \infty \\
&\bar{\phi}(Z, 0) = \begin{cases} \frac{\Phi_0}{1-\Phi_0}\mathrm{e}^{\frac{Z}{2}}, & 0 < Z \le Pe\left(1 - \Phi_0\right) \\ 0, & Z > Pe\left(1 - \Phi_0\right). \end{cases}
\end{aligned}. \quad (4.12)$$

A semi-explicit solution of (4.12) can be found in [7] and the interested reader is referred there for technical details. This semi-explicit solution consists of two integral contributions as shown below:

$$\bar{\phi}(Z,T) = \frac{\Phi_0}{2(1-\Phi_0)} \int_0^{Pe(1-\Phi_0)} \left\{ \frac{1}{\sqrt{\pi T}} \left[\mathrm{e}^{-(Z-Z')^2/4T} + \mathrm{e}^{-(Z+Z')^2/4T} \right] + \right.$$
$$\left. + \mathrm{e}^{T/4-(Z+Z')/2} \mathrm{erfc} \left[\frac{Z+Z'}{2\sqrt{T}} - \frac{1}{2}\sqrt{T} \right] \right\} \mathrm{e}^{\frac{Z'}{2}} dZ' \tag{4.13}$$

where erfc is the complementary error function defined in [1]. The original distribution $\phi(z,t)$ can be recovered from (4.13) using the identity

$$\phi(z,t) = \phi_p \left[\frac{\bar{\phi}(Z,T)}{\mathrm{e}^{Z/2+T/4} + \bar{\phi}(Z,T)} \right] \tag{4.14}$$

along with

$$z = \frac{1}{Pe} \int_0^Z \Phi^*(Z^{'},T)\, dZ^{'}, \tag{4.15}$$

where $\Phi^* = 1 + \bar{\phi}(Z,T)\mathrm{e}^{-(Z/2+T/4)}$. The solution for $\phi(z,t)$ is therefore given parametrically through $\phi(Z,T)$, $z(Z,T)$ and $t = T/Pe^2$.

We briefly comment on the generalization of this method to the case $0 < \chi < 1$, *i.e.* when the boundary condition (4.3) is given by

$$\frac{D_0}{(1-\phi/\phi_p)^2}\phi_z + \chi V \phi = 0 \text{ on } z = 0. \tag{4.16}$$

Using the same change of variables as in (4.6), one can show that the transformed problem is now given by

$$\begin{aligned}
&\frac{\partial \Phi^*}{\partial t} - (1-\chi)Pe\Phi_0^*(t) = \frac{\partial}{\partial z^*}\left[\Phi^*_{z^*} + Pe\,(\Phi^* - 1)\right] \\
&\Phi^*_{z^*} + \chi Pe\,(\Phi_0^*(t) - 1) = 0 \quad \text{on } z^* = 0 \\
&\Phi^* \to 1 \quad z^* \to \infty \\
&\Phi^*(z^*,0) = \begin{cases} \frac{1}{1-\Phi_0}, & 0 < z^* \le 1-\Phi_0, \\ 1, & z^* > 1-\Phi_0 \end{cases}
\end{aligned} \tag{4.17}$$

where χ is a constant and $\Phi_0^*(t) = \Phi^*(0,t)$ is the particle volume fraction at the interface $z = 0$ and is, therefore, a function of time only. The problem (4.17) is more involved than the standard Lie-Bäcklund transformation problem in (4.10) and we plan to study the corresponding analytic solutions in future work.

5. Results and discussion. In this section, we present the modelling results for Watanabe's experiment [41]. The integrals in (4.13) were calculated using MATLAB's Lobatto quadrature function quadl. Solutions to (3.4)–(3.8) were also obtained numerically using the method of lines [21]. Exact agreement with (4.13) was verified in the case $\chi = 1$. Figure 5.1(a)–(e) shows results of the model for the case $L = 4\,\mathrm{cm}$, $G_T = 0.5\,^\circ\mathrm{C/m}$, $\phi_0 = 0.5$, $V = 0.15\,\mu\mathrm{m/s}$ and $\chi = 1$, corresponding to the dimensionless parameters $Pe = 160$ and $\Phi_0 = 0.78$. For clarity of presentation the results

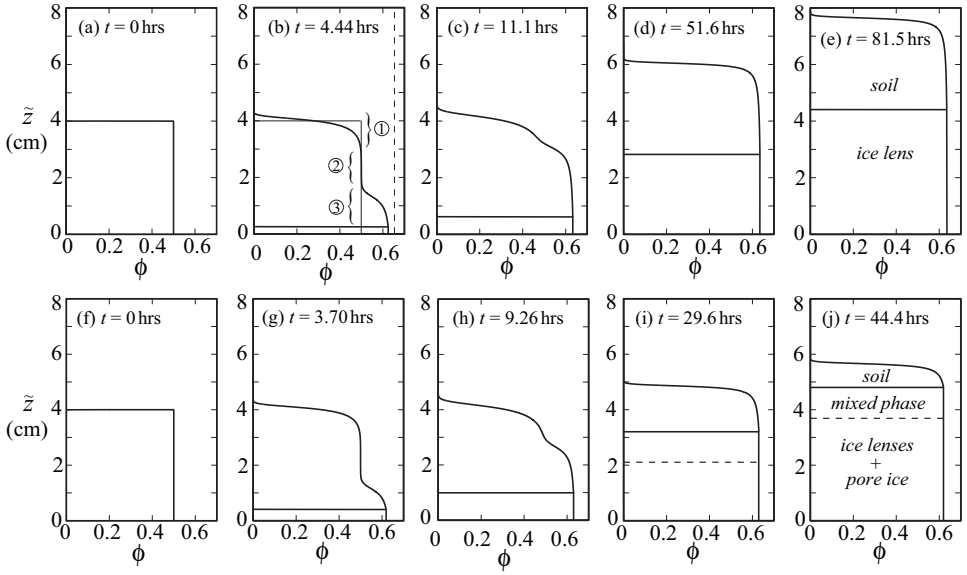

FIG. 5.1. *Plots of $\phi(z,t)$ in the case $\chi = 1$, (a)–(e), and $\chi = 0.5$, (f)–(j). In (b)–(e) and (g)–(j) the horizontal solid line designates the 0° C isotherm, while the dashed line in (i) and (j) designates the breakthrough temperature T_E isotherm.*

are plotted in the cell frame $\tilde{z} = z + Vt$. Thus figure 5.1(a) shows the initial state of the soil, while in figures (b)–(e) the temperature at the base $\tilde{z} = 0$ is being lowered at the rate $G_T V$. Since $\chi = 1$ a single ice lens forms at $\tilde{z} = 0$ and pushes ahead the soil particles. Two distinct regimes of behaviour occur.

In the *consolidation* regime, figures 5.1(b) and (c), the soil consolidates as the ice forms. During this period the water which feeds the ice layer comes from the consolidated soil ahead of the ice–soil boundary and no heave occurs. In reality we would expect a small amount of heave to occur owing to the volume expansion of ice. However, as noted in the introduction, volumetric expansion is not essential to frost heave and has been neglected in this work.

In the *heaving regime*, figures 5.1(d) and (e), the soil is fully consolidated. During this period the ice grows by displacing (heaving) the entire column of soil. The water which feeds the ice layer in this case comes from the external reservoir. To quantify the amount of heave we define the upper surface of the soil as the point at which $\phi = \phi_0$. With this definition the height of the soil actually decreases in figures 5.1(b) and (c). This is due to swelling, where the preconsolidated soil expands upward into the water reservoir. To distinguish between swelling and heave, we have superimposed the initial undisturbed soil profile on figure 5.1(b). The dashed line shows the maximum close-packing concentration ϕ_p. At $t = 4.44$hrs three distinct regions can be discerned in the figure: (1) a swelling region where the upper surface of the soil has diffused into the water reservoir, (2) an undisturbed portion of soil, and (3) a consolidated soil layer above the ice interface. Frost heave commences only after figure 5.1(c), when the consolidated layer reaches the surface of the soil. Thus the present model can simulate both swelling and heaving processes simultaneously.

In the case $0 < \chi < 1$ the equations were solved numerically. In figures 5.1(f)–(j) $V = 0.3\,\mu$m/s, and all other parameter values are unchanged, leading to $Pe = 320$

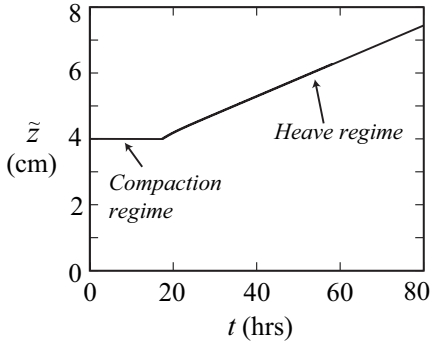

FIG. 5.2. *Height of the soil as a function of time.*

and $\chi = 0.5$. At this higher freezing rate a mixed phase region forms containing both unfrozen soil and segregated ice. Figures (g) and (h) show the consolidation regime, while (i) and (j) illustrate the heaving regime. In (i) and (j) the dashed line shows the T_E isotherm determined by equation (3.3); below the dashed line the soil contains pore ice. The T_E isotherm is not shown in figures 5.1(a)–(e) because in that case the soil is entirely pushed ahead by the ice and remains unfrozen. Only in the case $\chi < 1$ does the soil move to lower temperatures allowing for ice breakthrough to occur. Note that if the soil was initially preconsolidated to the breakthrough pressure $11\gamma/R$ (or larger values) ice would simply invade the pore space and no heave would occur (maximum frost heave pressure).

The heaving of the soil is shown in figure 5.2. We ignore the effects of swelling during the consolidation phase and set the heave rate to zero. During the heaving phase, the heave magnitude is obtained by tracking the highest point at which $\phi \geq \phi_0$. After an initial transient the heave is a linear function of time. Figure 5.2 shows the heave for both cases in figure 5.1, $V = 0.15\,\mu$m/s and $V = 0.3\,\mu$m/s, and the curves are almost indistinguishable. This result, that the heave rate is independent of the rate of freezing, is in agreement with field and laboratory observations of frost heave [4, 26]. An explanation for this result can be obtained by writing the governing equations in a frame of reference fixed with respect to the soil/water interface (moving at the heaving rate u) as

$$\frac{\partial \phi}{\partial t} = \frac{\partial}{\partial z}\left(D(\phi)\frac{\partial \phi}{\partial z} + u\phi \right), \tag{5.1}$$

$$\chi \phi V = -D(\phi)\frac{\partial \phi}{\partial z}. \tag{5.2}$$

At steady state $\partial\phi/\partial t = 0$ so that (5.1) and (5.2) can be combined to give $\chi V = u + c$ where c is a constant. Since $\chi \sim V^{-1}$, u is independent of V.

In this work we have developed a mathematical model of frost heave that captures several essential features of the phenomenon, including the drop in ice fraction with increasing V, the consolidation of the unfrozen soil, and the mutual independence of the heave rate and the rate of freezing. With appropriate diffusivities we have solved the equations analytically and numerically. The analytic solution demonstrates that Lie-Bäcklund transformations can be applied to the field of frost heave dynamics, and we expect such transformations to be of use in obtaining solutions to more complex cases than considered here.

Acknowledgments. This research was supported by the King Abdullah University of Science and Technology (KAUST), Award No. KUK-C1-013-04.

REFERENCES

[1] M. Abramowitz and I. A. Stegun, *Handbook of Mathematical Functions with Formulas, Graphs, and Mathematical Tables*, Dover, New York, 1972.

[2] D. A. Barry and G. C. Sander, *Exact solutions for water infiltration with an arbitrary surface flux or nonlinear solute adsorption*, Water Resour. Res., 27 (1991), pp. 2667–2680.

[3] D. A. Barry and G. Sposito, *Analytical solution of a convection-dispersion model with time-dependent transport coefficients*, Water Resour. Res., 25 (1989), pp. 2407–2416.

[4] G. Beskow, *Soil freezing and frost heaving with special attention to roads and railroads*, The Swedish Geological Society, C, no. 375, Year Book no. 3. Technological Institute, Northwestern University. Reprinted in *Historical Perspectives in Frost Heave Research*, P. B. Black and M. J. Hardenberg, eds., CRREL Special Report 91-23, 1991, pp. 37–157.

[5] S. C. Brown, *Soil Freezing*, PhD Thesis, University of Reading, UK, 1984.

[6] S. C. Brown and D. Payne, *Frost action in clay soils. II. Ice and water location and suction of unfrozen water in clays below 0°C*, J. Soil Sci., 41 (1990), pp. 547–561.

[7] H. S. Carslaw and J. C. Jaeger, *Conduction of Heat in Solids. 2nd Edition*, Oxford University Press, UK, 1986.

[8] J.-M. Chen, Y.-C. Tan, C.-H. Chen and J. Y. Parlange, *Analytical solutions for linearized Richards equation with arbitrary time-dependent surface fluxes*, Water Resour. Res., 37 (2001), pp. 1091–1093.

[9] J. G. Dash, A. W. Rempel and J. S. Wettlaufer, *The physics of premelted ice and its geophysical consequences*, Rev. Mod. Phys., 78 (2006), pp. 695–741.

[10] K. E. Davis, W. B. Russel and W. J. Glantschnig, *Settling suspensions of colloidal silica: Observations and X-ray measurements*, J. Chem. Soc. Faraday Trans., 87 (1991), pp. 411–424.

[11] K. E. Davis and W. B. Russel, *An asymptotic description of transient settling and ultrafiltration of colloidal dispersions*, Phys. Fluids A, 1 (1989), pp. 82–100.

[12] A. C. Fowler, *Secondary frost heave in freezing soils*, SIAM J. Appl. Maths., 49 (1989), pp. 991–1008.

[13] A. S. Fokas, Y. C. Yortsos, *On the exactly solvable equation* $S_t = [(\beta S+\gamma)^{-2}S_x]_x + \alpha(\beta S+\gamma)^{-2}S_x$ *occurring in two-phase flow in porous media*, SIAM J. Appl. Math., 42 (1982), pp. 318–332.

[14] J. J. Guo and J. A. Lewis, *Aggregation effects on the compressive flow properties and drying behavior of colloidal silica suspensions*, J. Am. Ceram. Soc., 82 (1999), pp. 2345–2358.

[15] J. L. Hilden and K. P. Trumble, *Numerical analysis of capillarity in packed spheres: Planar hexagonal-packed spheres*, J. Colloid Interface Sci., 267 (2003), pp. 463–474.

[16] H. E. Huppert and M. G. Worster, *Dynamic Solidification of a Binary Melt*, Nature, 314 (1985), pp. 703–707.

[17] K. A. Jackson, D. R. Uhlmann and B. Chalmers, *Frost heave in soils*, J. Appl. Phys., 37 (1966), pp. 848–852.

[18] J.-M. Konrad and C. Duquennoi, *A model for water transport and ice lensing in freezing soils*, Water Resour. Res., 29 (1993), pp. 3109–3124.

[19] J.-M. Konrad, *Frost susceptibility related to soil index properties*, Can. Geotech. J., 36 (1999), pp. 403–417.

[20] J. S. Langer, *Instabilities and pattern formation in crystal growth*, Rev. Mod. Phys., 52 (1980), pp. 1–28.

[21] H. S. Lee, C. J. Matthews, R. D. Braddock, G. C. Sander and F. Gandola, *A MATLAB method of lines template for transport equations*, Environ. Modell. Softw., 19 (2004), pp. 603–614.

[22] P. F. Low, D. M. Anderson and P. Hoekstra, *Some thermodynamic relationships for soils at or below the freezing point. 1. Freezing point depression and heat capacity*, Water Resour. Res., 4 (1968), pp. 379–394.

[23] R. D. Miller, *Frost heaving in non-colloidal soils*, in Proceedings of the 3rd International Conference on Permafrost, National Research Council of Canada, Edmonton, Alberta, 1978, pp. 708–713.

[24] K. O'Neill and R. D. Miller, *Exploration of a rigid ice model of frost heave*, Water Resour. Res., 21 (1985), pp. 281–296.

[25] E. Penner, *Frost heaving in soils*, in Proceedings of the International Conference on Per-

mafrost, National Research Council, Lafayette, Indiana, 1963, pp. 197–202.
[26] E. Penner, *Influence of freezing rate on frost heaving*, Highway Res. Rec., 1972, pp. 56–64.
[27] S. S. L. Peppin, A. Majumdar & J. S. Wettlaufer, *Morphological instability of a non-equilibrium ice–colloid interface*, Proc. Roy. Soc. Lond. A, 466 (2010), pp. 177–194.
[28] S. S. L. Peppin, J. A. W. Elliott and M. G. Worster, *Solidification of colloidal suspensions*, J. Fluid Mech., 554 (2006), pp. 147–166.
[29] S. S. L. Peppin, J. S. Wettlaufer and M. G. Worster, *Experimental verification of morphological instability in freezing aqueous colloidal suspensions*, Phys. Rev. Lett., 100 (2008), 238301.
[30] S. S. L. Peppin, M. G. Worster and J. S. Wettlaufer, *Morphological instability in freezing colloidal suspensions*, Proc. Roy. Soc. Lond. A, 463 (2007), pp. 723–733.
[31] E. Penner, *Experimental pressure studies of frost heave mechanisms and the growth-fusion behavior of ice*, in Proceedings of the Second International Conference on Permafrost, National Research Council, Yakutsk, USSR, 1973, pp. 377–384.
[32] C. Rogers, M. P. Stallybrass and D. L. Clements, *On 2 phase filtration under gravity and with boundary infiltration – application of a Bcklund transformation*, Nonlinear Anal. Theory Methods Appl., 7 (1983), pp. 785–799.
[33] A. W. Rempel and M. G. Worster, *The interaction between a particle and an advancing solidification front*, J. Cryst. Growth, 205 (1999), pp. 427–440.
[34] A. W. Rempel, J. S. Wettlaufer and M. G. Worster, *Premelting dynamics in a continuum model of frost heave*, J. Fluid Mech., 498 (2004), pp. 227–244.
[35] W. B. Russel, D. A. Saville and W. R. Schowalter, *Colloidal Dispersions*, Cambridge University Press, UK, 1989.
[36] N. O. Shanti, K. Araki and J. W. Halloran, *Particle redistribution during dendritic solidification of particle suspensions*, J. Am. Ceram. Soc., 89 (2006), pp. 2444–2447.
[37] S. Taber, *Frost heaving*, J. Geol., 34 (1929), pp. 428–461.
[38] D. R. Uhlmann, B. Chalmers and K. A. Jackson, *Interaction between particles and a solid–liquid interface*, J. Appl. Phys., 35 (1964), pp. 2986–2993.
[39] K. Watanabe and M. Mizoguchi and T. Ishizaki and M. Fukuda, *Experimental study on microstructure near freezing front during soil freezing*, in Proceedings of the International Symposium of Ground Freezing, 1997, pp. 187–194.
[40] K. Watanabe and M. Mizoguchi, *Ice configuration near a growing ice lens in a freezing porous medium consisting of micro glass particles*, J. Cryst. Growth, 213 (2000), pp. 135–140.
[41] K. Watanabe, *Relationship between growth rate and supercooling in the formation of ice lenses in a glass powder*, J. Cryst. Growth, 237-239 (2002), pp. 2194–2198.
[42] P. J. Williams and M. W. Smith, *The Frozen Earth: Fundamentals of Geocryology*, Cambridge University Press, UK, 1989.
[43] M. G. Worster, *Solidification of Fluids*, in Perspectives in Fluid Dynamics, G. K. Batchelor, H. K. Moffatt and M. G. Worster, eds., Cambridge University Press, U. K, 2000, pp. 393–446.
[44] D.-M. Zhu, O. F. Vilches, J. G. Dash, B. Sing and J. S. Wettlaufer, *Frost heave in argon*, Phys. Rev. Lett., 85 (2000), pp. 4908–4912.

RECENT REPORTS

31/09	Stochastic neural field theory and the system-size expansion	Bressloff
32/09	A Hamiltonian Krylov-Schur-type method based on the symplectic Lanczos process	Benner Faßbender Stoll
33/09	Nematic liquid crystals : from Maier-Saupe to a continuum theory	Ball Majumdar
34/09	Tangent unit-vector fields: nonabelian homotopy invariants and the Dirichlet energy	Majumdar Robbins Zyskin
35/09	A metabolite-sensitive, thermodynamically-constrained model of cardiac cross-bridge cycling: Implications for force development during ischemia	Tran Smith Loiselle Crampin
36/09	Modelling bacterial behaviour close to a no-slip plane boundary: the influence of bacterial geometry	Shum Gaffney Smith
37/09	Optimal L2-error estimates for the semidiscrete Galerkin approximation to a second order linear parabolic initial and boundary value problem with nonsmooth initial data	Goswami Pani
38/09	Optimal L2 estimates for semidiscrete Galerkin methods for parabolic integro-differential equations with nonsmooth data	Goswami Pani Yadav
39/09	Spatially structured oscillations in a two-dimensional excitatory neuronal network with synaptic depression	Kilpatrick Bressloff
40/09	Stationary bumps in a piecewise smooth neural field model with synaptic depression	Kilpatrick Bressloff
41/09	Homogenization for advection-diffusion in a perforated domain	Haynes Hoang Norris Zygalakis
42/09	Fast stochastic simulation of biochemical reaction systems by alternative formulations of the Chemical Langevin Equation	Melykuti Burrage Zygalakis
43/09	Pseudoreplication invalidates the results of many neuroscientific studies	Lazic
44/09	Cardiac cell modelling: Observations from the heart of the cardiac physiome project	Finka *et al.*

45/09	A Hybrid Radial Basis Function - Pseudospectral Method for Thermal Convection in a 3-D Spherical Shell	Wright Flyer
46/09	Refining self-propelled particle models for collective behaviour	Yates Baker Erban Maini
47/09	Stochastic Partial Differential Equations as priors in ensemble methods for solving inverse problems	Potsepaev Farmer Aziz
48/09	DifFUZZY: A fuzzy spectral clustering algorithm for complex data sets	Cominetti *et al.*
01/10	Fluctuations and instability in sedimentation	Guazzelli Hinch
02/10	Determining the equation of state of highly plasticised metals from boundary velocimetry	Hinch
03/10	Stability of bumps in piecewise smooth neural elds with nonlinear adaptation	Kilpatrick Bressloff
04/10	Random intermittent search and the tug–of–war model of motor–driven transport	Newby Bressloff
05/10	Ergodic directional switching in mobile insect groups	Escudero *et al.*
06/10	Derivation of a dual porosity model for the uptake of nutrients by root hairs	Zygalakis Roose

Copies of these, and any other OCCAM reports can be obtained from:

Oxford Centre for Collaborative Applied Mathematics
Mathematical Institute
24 - 29 St Giles'
Oxford
OX1 3LB
England
www.maths.ox.ac.uk/occam